INSTITUT DE FRANCE
Académie des sciences

Comptes Rendus

Mécanique

Jiaxiang Luo, Yihe Xu, Yu Zhong, Jidong Teng, Wen Yao, Lei Hao and Chenlei Kang

Molecular dynamics analysis of wetting behavior of nano water drops on quartz sand surface

Volume 349, issue 3 (2021), p. 485-499

Published online: 20 October 2021

https://doi.org/10.5802/crmeca.95

Les Comptes Rendus. Mécanique *sont membres du Centre Mersenne pour l'édition scientifique ouverte*
www.centre-mersenne.org
e-ISSN : 1873-7234

Comptes Rendus
Mécanique
2021, 349, nº 3, p. 485-499
https://doi.org/10.5802/crmeca.95

Short paper / *Note*

Molecular dynamics analysis of wetting behavior of nano water drops on quartz sand surface

Jiaxiang Luo [a], **Yihe Xu** [b], **Yu Zhong** [c], **Jidong Teng** [*, c], **Wen Yao** [a], **Lei Hao** [d] **and Chenlei Kang** [e]

[a] College of Aerospace Science and Engineering, National University of Defense Technology, Changsha 410073, China

[b] Department of Geotechnical Engineering, Tongji University, Shanghai 200092, China

[c] School of Civil Engineering, Central South University, Changsha 410075, China

[d] Tangshan Port Industrial Group Co., Ltd., Tangshan 063000, China

[e] Southwest Survey and Design Group Co., Ltd., China Railway Siyuan Group, Kunming 650200, China

Current address: Railway Campus of Central South University, Shaoshan South Road No. 68, Changsha, Hunan Province, 410075, China (J. Teng)

E-mails: luojiaxiang22@163.com (J. Luo), 1930166@tongji.edu.cn (Y. Xu), zhongyu@csu.edu.cn (Y. Zhong), jdteng@csu.edu.cn (J. Teng), wendy0782@126.com (W. Yao), hl15512552798@163.com (L. Hao), 1176230126@qq.com (C. Kang)

Abstract. The wettability mechanism of soil–water interfaces is of significant importance in geotechnical engineering. However, the effect of different contact angles on unsaturated sand soil behavior has been less understood. In this study, the wetting behavior of nano water droplets on various silica substrates is investigated using molecular dynamics. Seventeen groups of simulation systems with different interaction potential energies (ε_{Si} = 0.008, 0.04, 0.2, 0.4, 0.6, 0.8, 1, 2 kcal/mol) and temperatures (T = 273, 298, 323, 353 K) are conducted. The results show that the contact angles varies intensively with interaction potential energies from 108.5° to 18.1°, which indicates a transition from hydrophobic to hydrophilic and wettability enhancement along with the increase of interaction potential energy. Simulation results also show that contact angles increase with the increase of temperature, whatever the hydrophobic or hydrophilic of the silica surface. Such phenomena are interpreted from the perspective of microstructure, along with the performance of macrostructure. In addition, results show that the contact angles are independent of the thickness and width (length) of silica substrate.

Keywords. Nano water droplets, Quartz sand, Silica, Wettability, Contact angle, Molecular dynamics.

Manuscript received 1st September 2020, revised 3rd September 2021, accepted 7th September 2021.

* Corresponding author.

1. Introduction

Wetting phenomena on a solid surface is a common and vital feature in many aspects of environmental and geotechnical engineering. It is found that a number of mechanisms of sand soil, such as shear strength and consolidation characteristics, are strongly dependent on the wettability between water and sand soil particles [1,2]. In turn, due to the various wettability of sand soil, dangerous situations occur, for instance, uneven settlement of soil, mud pumping, slope collapse in practical engineering [3,4]. Thus, a detailed understanding of soil–water interface is in a center of interest.

According to the Young–Laplace equation [5], contact angle θ is one of the essential quantification criteria of wettability [6, 7]. If the contact angle θ between a liquid and a solid surface is more than 90°, the surface is hydrophobic. Otherwise, the surface is hydrophilic [8, 9]. It is generally assumed that the contact angles of soil surfaces are constant and mostly zero in unsaturated soil mechanics for the reason of the high surface energy and simplicity's sake from a macroscopic perspective [10–12]. However, with the increasing water content of sand soil, the soil–water–air interphase (menisci) between sand particles shows various contact angles from a microscopic perspective [13]. Consequently, the effect of contact angles on the unsaturated sand soil behavior is far from being thoroughly understood. Therefore, it is indispensable to research contact angles of sand soil and quantify their effects of wettability on unsaturated soil behavior, and thus optimize practical engineering problems induced by wetting phenomena.

Experiments have been performed to monitor the surface tensions using a variety of methods on the macroscopic scale, for instance, the capillary rise method [14], the sessile drop method [15], and Wilhelmy method [16]. Meanwhile, a series of calculation methods have been proposed to measure the contact angles, for example, the snake method [17], the Young–Laplace equation numerical synthesis method [18], and the low-bond symmetric droplet shape analysis method (LBDSA) [19]. Determination of the contact angles for soil material is usually difficult because the measurements are affected by various factors such as temperature, relative humidity, particle shape and size, surface heterogeneity and roughness, etc. [20]. Thus, those factors need to be quantified by efficient experimental or numerical methods.

Quantifying the wettability character of a solid surface requires an understanding of the microscopic wetting behavior of the surface. Molecular dynamics (MD) simulation has been recognized as a useful tool in the investigation of microscopic complex physical mechanisms on solid surfaces. In recent years, several molecular simulations have been performed in the study of surface properties of solid matter simulating interactions of liquid nano droplets with various surfaces. Sergi *et al.* [21] applied the MD method to simulate the wetting process about pure water with an initial radius of droplets of 2–8 Å on a graphite surface, and calculated the contact angle at equilibrium state. Xu *et al.* [22] studied the process of nano water droplets wetting surfaces with different energy and found the relationship between solid–liquid interaction strength and contact angle of nano water droplets. Wu *et al.* [23] simulated the process of nano water droplets wetting the solid gold surface. The results showed that the increase of temperature was beneficial to the improvement of wettability. Niu and Tang [24] simulated the static and dynamic processes of nano water droplets wetting matrix graphene. The results showed that the height and phase area fraction of the square column would affect the contact state of the droplets. Jeong *et al.* [25] simulated the static and dynamic processes of nano water droplets wetting smooth and rough surfaces, respectively. Ambrosia *et al.* [26] simulated the wetting process of nano water droplets on the surface of graphite arrays. The results showed that the contact angle of nano water droplets increased first and then remained unchanged with the increase of the height of graphite arrays. It is noted that the researches on wettability mainly focus on the wetting behavior of different

gaseous or liquid molecules on the contact surfaces of metals. The wetting process of water molecules on the surface of silica has not been studied clearly. Moreover, the study of molecular dynamics from a geotechnical point of view is relatively deficient.

Among the rich groups of natural sand, silica sand has an important role because of its high abundance in nature, advantageous thermal properties, and relatively pure chemical composition, silica (SiO_2). To promote its application in the geotechnical engineering community, molecular dynamics simulations are adopted in this study to explore the wetting behavior of silica soil surfaces. Meanwhile, a series of wetting process simulations of nano water droplets on silica surfaces are conducted by the large-scale atomic/molecular massively parallel simulator (LAMMPS) and visualized by visual molecular dynamics (VMD) to investigate the contact angles. In this paper, we investigate the variation tendency of the contact angles, droplet heights, and vapor–liquid interface thicknesses of the moving nano water droplet on the silica soil surface with different thicknesses, lengths, widths, interaction potential energies, and temperatures. The underlying physical mechanisms of wetting processes and their implications on silica soil mechanics are discussed further in detail.

2. Simulation details

2.1. *Interatomic force fields*

In order to calculate the interatomic potentials in the simulation system mathematically, it is necessary to define force fields between various types of atoms. We employ a potential energy function compatible with the consistent valence force field (CVFF) [27, 28], which is based on a combination of ab initio data and the consistent force field [29, 30] based on the same ab initio data as the ab initio shell model potential [31]. In the CVFF force field, the total potential energy of the system can be classified as the Lennard–Jones (L–J) potential energy in the short range [32] and the Coulomb potential energy in the long range. The functional form is used as (1).

$$\begin{aligned} U^S &= U_e^S + U_{\mathrm{LJ}}^S \\ &= \sum_{i=1}^{N}\sum_{j>i}^{N}\sum_{a=1}^{n}\sum_{b=1}^{n}\frac{q_i^a q_i^b}{4\pi\varepsilon_R r_{ij}^{ab}} + \sum_{i=1}^{N}\sum_{j>i}^{N} 4\varepsilon_{\mathrm{O}}\left[\left(\frac{\sigma_{\mathrm{O}}}{r_{ij}^{\mathrm{OO}}}\right)^{12} - \left(\frac{\sigma_{\mathrm{O}}}{r_{ij}^{\mathrm{OO}}}\right)^{6}\right], \end{aligned} \tag{1}$$

where U^S is the total potential energy of the system, kcal/mol. U_e^S is the long-range Coulomb potential energy representing the electrostatic energy between point charges, kcal/mol. U_{LJ}^S is the short-range L–J potential energy, which represents Van der Waals energy defined by a conventional function, kcal/mol, N is the number of molecules, n is the number of points of action of molecules that are electrostatically charged within any water molecule in the system, i and j are two different types of the water molecule, a and b are the points where the molecules are subjected to Coulomb potential, q_i^a and q_j^b are the partial atomic charges of point a and b, r_{ij}^{ab} is the distance between the point a in molecule i and the point b in molecule j, m; ε_R is dielectric permittivity of vacuum which is equal to 8.854×10^{-12} F/m. The r_{ij}^{OO} is the distance between the two oxygen atoms in molecule i and molecule j, m; σ_{O} is the distance at which interaction energy of two oxygen atoms is minimal, Å; ε_{O} is the characteristic energy, kcal/mol.

For water molecules, all parameters are taken from the CVFF force field. The reference water model used in this study is the transferable intermolecular potential (TIP3P). The model has a single Lennard–Jones center representing an oxygen atom together with three charges arranged in a triangle [33]. All the nonbonding and bonding parameters are shown in Table 1.

The parameter q^{H} is the charge amount of hydrogen atoms, q^{O} is the charge amount of oxygen atoms, r_{OH} is the distance between hydrogen and oxygen atom (i.e., the bond length

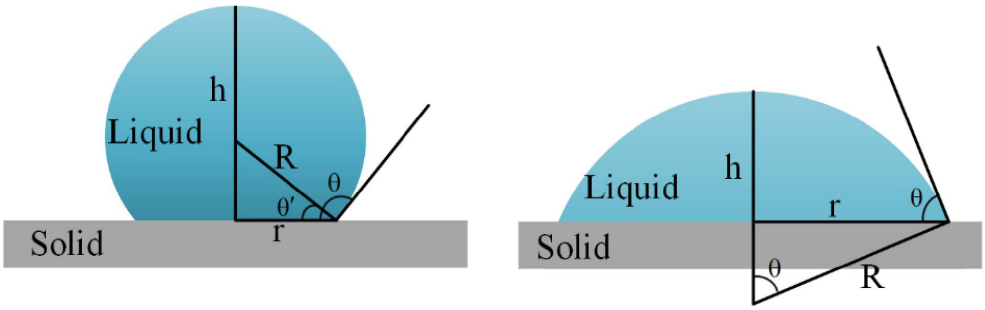

Figure 1. Geometry for inherency contact angle on the solid surface.

Table 1. Parameter values of the TIP3P model

σ_O/Å	ε_O/kcal/mol	q_H/e	q_O/e	θ/(°)	r_{OH}/Å
3.188	0.102	+0.415	−0.83	104.52	0.9572

of the O–H bond), θ is the angle between two O–H bonds (i.e., the bond angle of the O–H bond), σ_O is the distance at which interaction energy of two oxygen atoms is minimal, ε_O is the characteristic energy, e is the basic charge ($1e = 1.6 \times 10^{-19}$ C), and k_B is Boltzmann constant ($k_B = 1.3806 \times 10^{-23}$ J/K).

For a brief summary, the interactions of soil–soil and soil–water are modeled in the CVFF force field while the water–water interaction is modeled by the TIP3P water model. Since there are different atomic species, the van der Waals interactions parameters can be calculated by using the Lorentz–Berthelot mixing rule

$$\sigma_{AB} = \tfrac{1}{2}(\sigma_A + \sigma_B) \tag{2}$$

$$\varepsilon_{AB} = \sqrt{\varepsilon_A \varepsilon_B}, \tag{3}$$

where ε_A and ε_B are characteristic energy on action points A and B, respectively, kcal/mol. The σ_A and σ_B are distances at which interaction energy action points A and B is minimal, Å.

2.2. *Definition of contact angle*

In this paper, the contact angle (θ) of irregular microdroplets is calculated by following the determined geometric parameters, which are generally applicable to intersecting spheres and irregular shape microdroplets. The contact angle is defined by following the model method [34]. Here, we outline the method used in the calculation. Figure 1 shows two droplets on the surface (one with $\theta > 90°$ and the other one with $\theta < 90°$). When the contact angle $\theta < 90°$, $\cos\theta = (R - h)/R$. Similarly for $\theta > 90°$, $\cos\theta = -(h - R)/R$. Here h is the height of the droplet relative to the solid surface, and R is the radius of the sphere.

In the method, the calculation of contact angle (θ) can be summarized as the following equation:

$$\cos\theta = 1 - \frac{h}{R} \tag{4}$$

2.3. *Initial configuration*

As illustrated in Figure 2, the initial configuration is modeled as a nano droplet of water placed on the top of a silica slab. The simulation cell size is $200 \times 200 \times 500$ Å and is adjusted to be integer

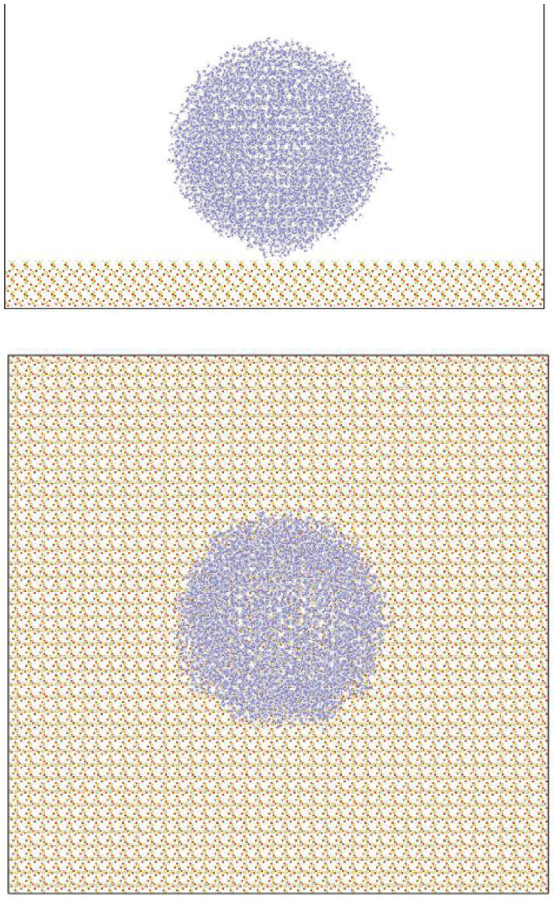

Figure 2. Initial configuration of the simulated system.

multiples of the lattice constants. The substrates are placed in the xy-plane of the simulation boxes, and the z-dimension of the simulation boxes is large enough to ensure that the atoms did not interact with their periodic images at any time. The smooth silica substrate consists of silicon and oxygen atoms, with a surface area of 200 Å × 200 Å. This surface area is more than two times larger than the cut-off distance, ensuring enough space for the water molecules to migrate during the simulation. The nano droplet water is 3 Å above the silica slab, which radius is 40 Å and randomly distributed in a spherical shape. Their initial velocities are generated according to a random number generator [35]. The number of water molecules filled in the cuboid is calculated to make the initial density of the nano droplet water equal to that of liquid water. In the whole process of simulation, the silica wall surface applies a rigid wall model [36], which can keep the wall surface fixed. This fixing does not affect the contact angle and reduces the computation time [37]. The velocity and interaction force between solid atoms can be neglected to reduce the simulation time and improve the calculation efficiency.

2.4. *Simulation setup*

The simulation is performed using the LAMMPS simulation package. The system has periodic boundary conditions in the x- and y-directions, while fixed and mirror boundary conditions are

Table 2. Overview of the interaction potential energies and temperatures applied in the simulation systems

ε_O/kcal·mol^{-1}	Case	ε_{Si}/kcal·mol^{-1}	ε_{Si-O}/kcal·mol^{-1}	Temperature/K
0.102	1	0.008	0.0286	273
	2	0.008	0.0286	298
	3	0.008	0.0286	323
	4	0.008	0.0286	353
	5	0.04	0.0639	273
	6	0.04	0.0639	298
	7	0.04	0.0639	323
	8	0.04	0.0639	353
	9	0.8	0.2856	273
	10	0.8	0.2856	298
	11	0.8	0.2856	323
	12	0.8	0.2856	353
	13	0.2	0.1428	298
	14	0.4	0.2020	298
	15	0.6	0.2474	298
	16	1	0.3194	298
	17	2	0.4517	298

applied in the z-direction [8], and thus the surfaces expand to infinite surfaces during simulations. Two reflecting walls are placed on the top and bottom of the simulation cell, respectively, to prevent the loss of water molecules through these two boundaries by a LAMMPS command "wall/reflect". In terms of the capillary water in soils, the gravitational gradient has a small influence on the geometry of the meniscus [38], especially for the nanoparticles [39]. Therefore, gravity is neglected in the current simulations [40]. The Lennard–Jones interactions in short ranges are truncated at cut-off distances of 9.0 Å. The long-range interaction is determined by particle–particle particle–mesh (PPPM) method. The van der Waals parameters for the simulated silica surface are van der Waals radius of σ_{Si} = 4.05343 Å, σ_O = 2.85978 Å and energy well depth ε_{Si} = 0.04 kcal/mol, ε_O = 0.228 kcal/mol.

The energy well depth ε_{Si} and ε_O which indicate the interaction potential between the silica and water molecules are changed, and this is a common method to research wettability through changing contact angles [41–45]. This approach focuses purely on the theoretical relationship between water contact angle and interaction energy, which means the variation of contact angle only depends on energy well depth or interaction energy. Table 2 shows the different energy well depth or interaction energy used in the simulations. It is significant to keep the modeling principle in mind when discussing simulation results.

The SHAKE algorithm is applied to constrain bond vibration, length, and angle in water molecules. All simulations are set in an NVT ensemble (constant number, volume, and temperature), and the Woodcock method is applied to maintain the simulation temperature constant. Verlet algorithm is used to numerically integrate Newton's equations of motion with a time step of 1 fs. The total simulation lengths are 3 ns. The equilibration process are attained during first 1 ns while the molecular trajectories during the last 2 ns are recorded for the density distribution, statistical data, and the state images of some specific moments.

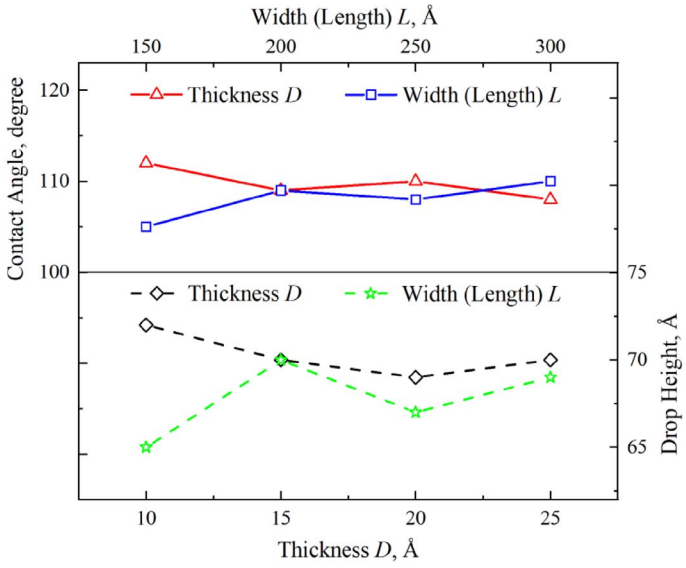

Figure 3. Influence of contact angles and total droplet heights on wall widths and thicknesses.

3. Results and discussions

3.1. *Effect of simulation parameters*

To investigate the effect of simulation parameters, a series of simulations with various lengths, widths, and thicknesses of silica walls are conducted in this part. The simulation cell size is 200 Å × 200 Å × 500 Å, including 24057 water molecules. We fix interaction energy $\varepsilon_{Si} = 0.04$ kcal/mol and temperature $T = 298$ K. Figure 3 shows the contact angle θ and total droplet height h under the silica wall thickness $D = 10, 15, 20, 25$ Å and width (length) $L = 150, 200, 250, 300$ Å. When the wall thickness and width change, the contact angles and vapor–liquid interface height fluctuate slightly. The contact angles are calculated to be $108.88 \pm 3.88°$, while the vapor–liquid interface heights are calculated to be 69 ± 3 Å. And the relative error is 3.56% and 4.35% for contact angle and the vapor–liquid interface height, respectively. Thus, it can be considered that the thickness, width, and length of the silica wall have little effect on the contact angle and the vapor–liquid interface height, so that this kind of effect can be ignored. It illustrates that the results are independent from the adopted numerical model. Considering the calculation efficiency and statistical error, we finally choose the wall width (length) $L = 200$ Å and wall thickness $D = 15$ Å in the following simulations.

3.2. *Effect of the potential energy of wall surface*

To investigate the impaction on water contact angle with potential energy, eight different interaction potential energies of silica walls have been considered, as illustrated in Table 2. Figure 4 shows the simulation systems in equilibrium state for various potential energy. As can be seen, the shapes of nano water droplets could be regarded as heterogeneous rounded, which is assumed in a statistical equilibrium state. Besides, several individual water molecules escape from nano water droplets into surrounding vapor or absorb to the silica surfaces, due to the phenomenon of molecular exchange and diffuse. Obviously, the nano water droplets become flatting with

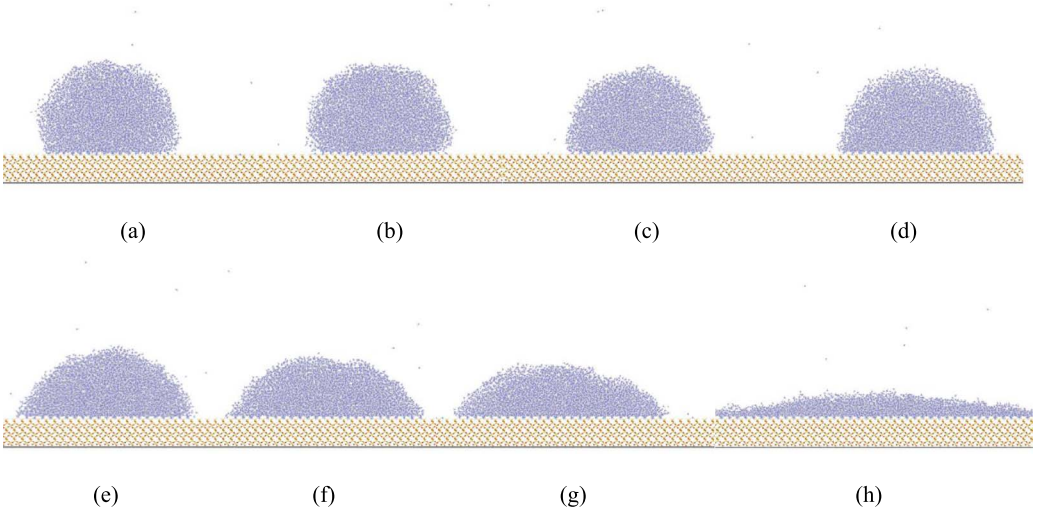

Figure 4. Snapshots of simulation systems at the equilibrium state for: (a) ε_{Si} = 0.008 kcal/mol; (b) ε_{Si} = 0.04 kcal/mol; (c) ε_{Si} = 0.2 kcal/mol; (d) ε_{Si} = 0.4 kcal/mol; (e) ε_{Si} = 0.6 kcal/mol; (f) ε_{Si} = 0.8 kcal/mol; (g) ε_{Si} = 1 kcal/mol; (h) ε_{Si} = 2 kcal/mol.

the potential energy increasing, which indicates that the silica wall turns hydrophobic to hydrophilic. The silica walls with potential energy ε_{Si} = 0.008–0.2 kcal/mol can be characterized as hydrophobic or non-wetting while the walls with potential energy ε_{Si} = 0.6–2 kcal/mol can be described as hydrophilic or wetting, and the walls with potential energy ε_{Si} = 0.4 kcal/mol can be claimed to be relatively neutral. The potential energy indicates the intensity of interaction energy between water molecules and silica wall atoms are closely related to surface tension and absorption mechanism of water. With small potential energy, the water molecules connect tightly as a compact entity maintaining a sphere form, which means the interactions within water droplets are stronger than interactions of water molecules and silica walls. With large potential energy, the absorption mechanism reduces most energy when water molecules approach the silica surface. Thus the counterbalance of tension and absorption mechanism maintains system energy minimum.

From the molecule dynamic simulation trajectories, time average density profiles of nano water droplets are calculated to interpret the simulation results when the simulation keeps in a statistical equilibrium state, as shown in Figure 5. In order to extract the contact angles better, a bin size of 180 × 80 Å in the x–z plane is employed to calculate. As illustrated in Figure 5, the nano water droplets could be clearly identified as regular rounded compared with snapshots in Figure 4, while the boundary between gas and liquid phase is more distinguished. However, it is interesting that the water droplets are not homogeneous, especially near the silica surface exists the higher density layers. In contrast, the densities near the vapor phase are much lower than normal water density in most areas of droplets.

The contact angle is measured from the density profiles of water molecules as suggested by Zhang *et al.* [46]. This method needs to determine the boundary of the liquid and vapor phase from time average density profiles. Figure 6 illustrates one-dimensional density profiles along the z-axis. Observed that the region closes to the silica surface shows a large and fluctuant density compared to the bulk water molecules, so this state can be regarded as a solid state or "quasi-solid" fluid, which is the dark blue region. This kind of phenomenon results from the dense packing of water molecules and is consistent with the observation in time average density profiles (Figure 4). As increasing height (z) those fluctuations decay, the density approaches a

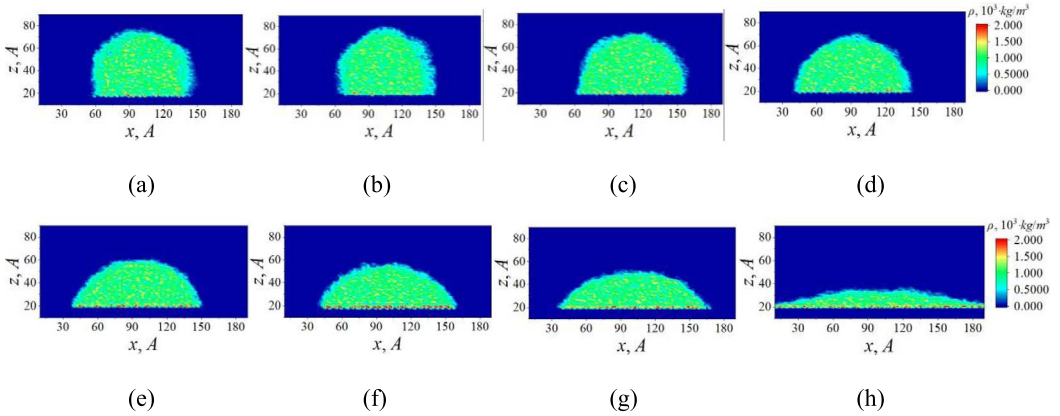

Figure 5. Time average density profiles of nano water droplet calculated at the equilibrium state for: (a) ε_{Si} = 0.008 kcal/mol; (b) ε_{Si} = 0.04 kcal/mol; (c) ε_{Si} = 0.2 kcal/mol; (d) ε_{Si} = 0.4 kcal/mol; (e) ε_{Si} = 0.6 kcal/mol; (f) ε_{Si} = 0.8 kcal/mol; (g) ε_{Si} = 1 kcal/mol; (h) ε_{Si} = 2 kcal/mol.

constant value relating to the water density, called liquid state, which is the cyan region. The vapor–liquid interface state is a transition zone between the liquid state and the vapor state, and the density drops sharply. The vapor zone, which is a light blue region, is mainly composed of gas, and its density is kept constant at 0 g/cm^3. The fit functions of one-dimensional density profiles can well approximate the vapor–liquid interface state. Various slices are selected to calculate the one-dimensional density because of the vacuum void among water molecules, which results in a minimum density of 0.2 g/cm^3. Thus, the water density at the boundary between liquid water and vapor can be assumed to be 0.2 g/cm^3.

To extract the contact angle of various potential energy from time average density profiles as shown in Figure 5, we determine the water droplet periphery as the contour line with 0.2 g/cm^3 in the one-dimensional density profiles using a least-squares circle fit through periphery as illustrated in Figure 7. The red broken line represents the height of the lowest water molecule layer, while the red circles represent the coordinates (x_i, z_i) along the water droplet periphery. The water droplet boundary can be considered as perfectly round, which mathematical equation is expressed in Figure 7. Thus according to the tangent line of the circle and the silica surface line, it is apparent to determine the contact angle.

Figure 8 shows the water contact angle as a function of the changing potential energy. The contact angle decreases linearly as the potential energy increases. It can be seen that the fitting curve matches the simulation results with a high significance. As mentioned above, there is a balance between surface tension and the absorption of water and silica wall to maintain the minimum system energy, which is the most stable state of the system. As a result, if the silica surface tension dissipates more energy than the absorption of water molecules, surface tension rejects the water molecules, so the contact area of the water droplet and silica surface becomes smaller, leading to a larger contact angle and the wettability of water on the silica surface decreases. Otherwise, with the high interaction potential energies, the water molecules are attracted by the silica surface and more water molecules are moving to the silica surface, leading to the decrease of the contact angle.

The vapor–liquid interface thickness and the total droplet height can be calculated as shown in Table 3. It can be seen that both of them decreased with the interaction potential energy increase, implied the smaller contact angles. This result can be a powerful verification of the mechanism of the contact angle.

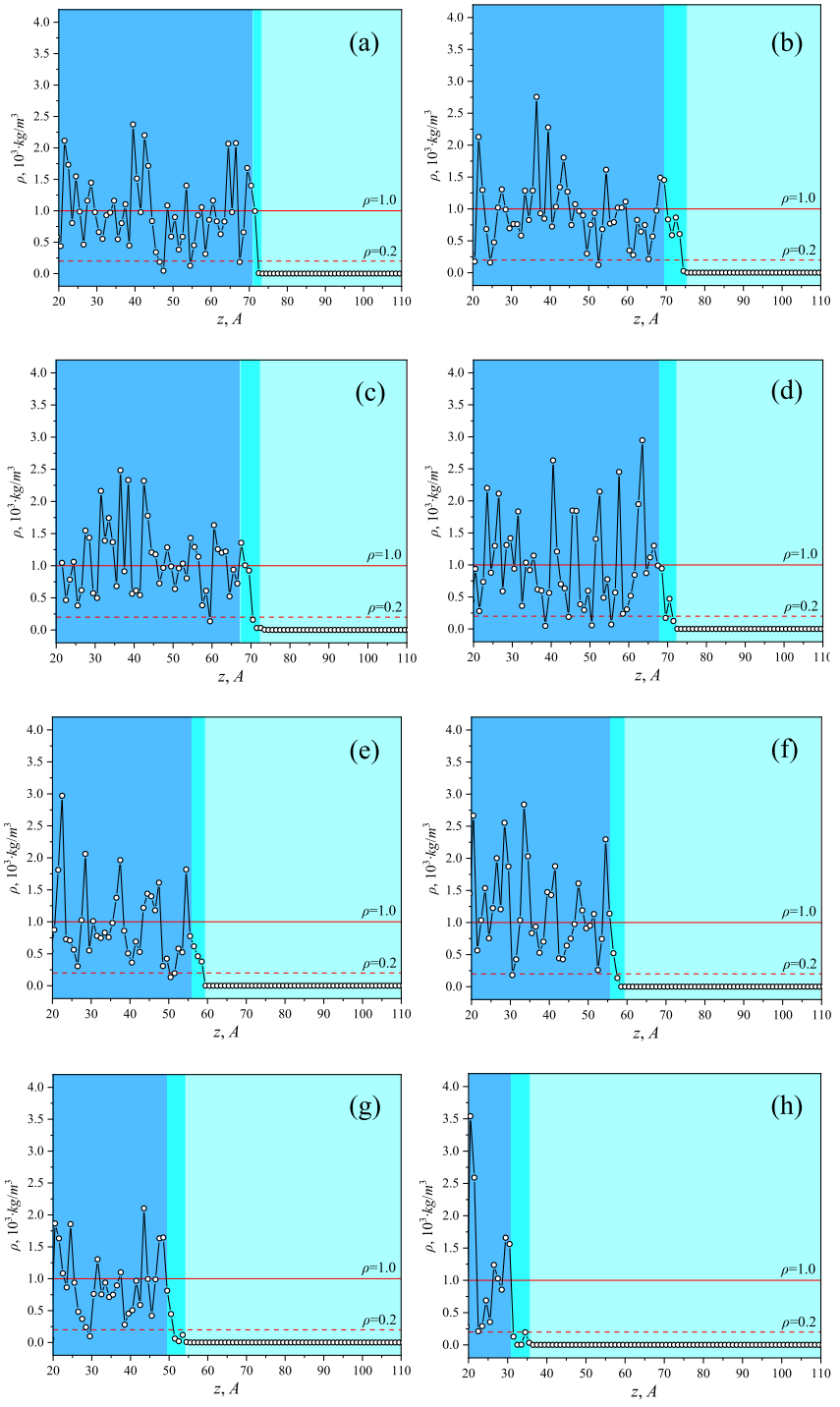

Figure 6. Density profiles along the centerline of the water droplet for: (a) ε_{Si} = 0.008 kcal/mol; (b) ε_{Si} = 0.04 kcal/mol; (c) ε_{Si} = 0.2 kcal/mol; (d) ε_{Si} = 0.4 kcal/mol; (e) ε_{Si} = 0.6 kcal/mol; (f) ε_{Si} = 0.8 kcal/mol; (g) ε_{Si} = 1 kcal/mol; (h) ε_{Si} = 2 kcal/mol.

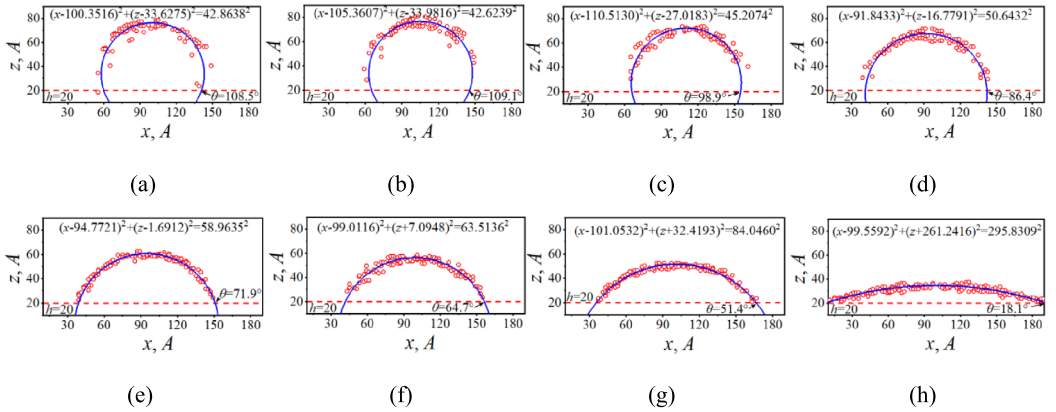

Figure 7. Determination of the contact angle of simulation systems for: (a) ε_{Si} = 0.008 kcal/mol; (b) ε_{Si} = 0.04 kcal/mol; (c) ε_{Si} = 0.2 kcal/mol; (d) ε_{Si} = 0.4 kcal/mol; (e) ε_{Si} = 0.6 kcal/mol; (f) ε_{Si} = 0.8 kcal/mol; (g) ε_{Si} = 1 kcal/mol; (h) ε_{Si} = 2 kcal/mol.

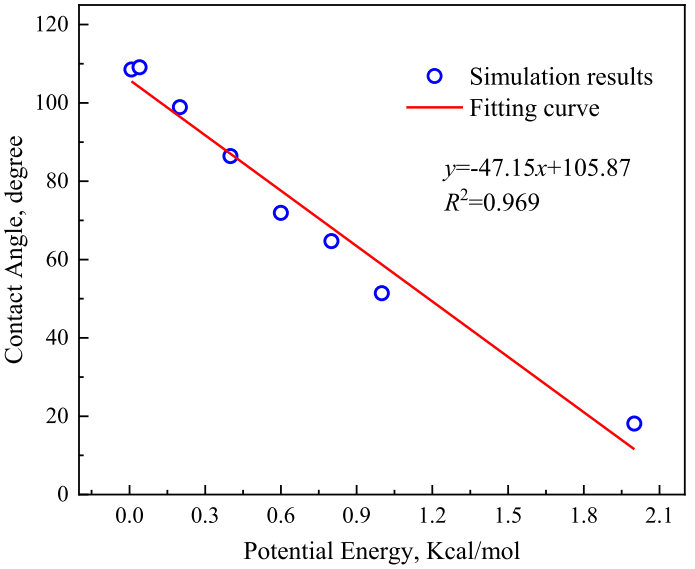

Figure 8. Contact angles of various potential energies.

Table 3. Vapor–liquid interface thickness and the total droplet height of various potential energies

Potential energy ε_{Si}/kcal·mol^{-1}	Thickness/Å	Height/Å
0.008	3	70.5
0.04	3	69.5
0.2	2.5	67
0.4	2.5	66.5
0.6	2	55.5
0.8	2	55
1	2	49.5
2	2	31

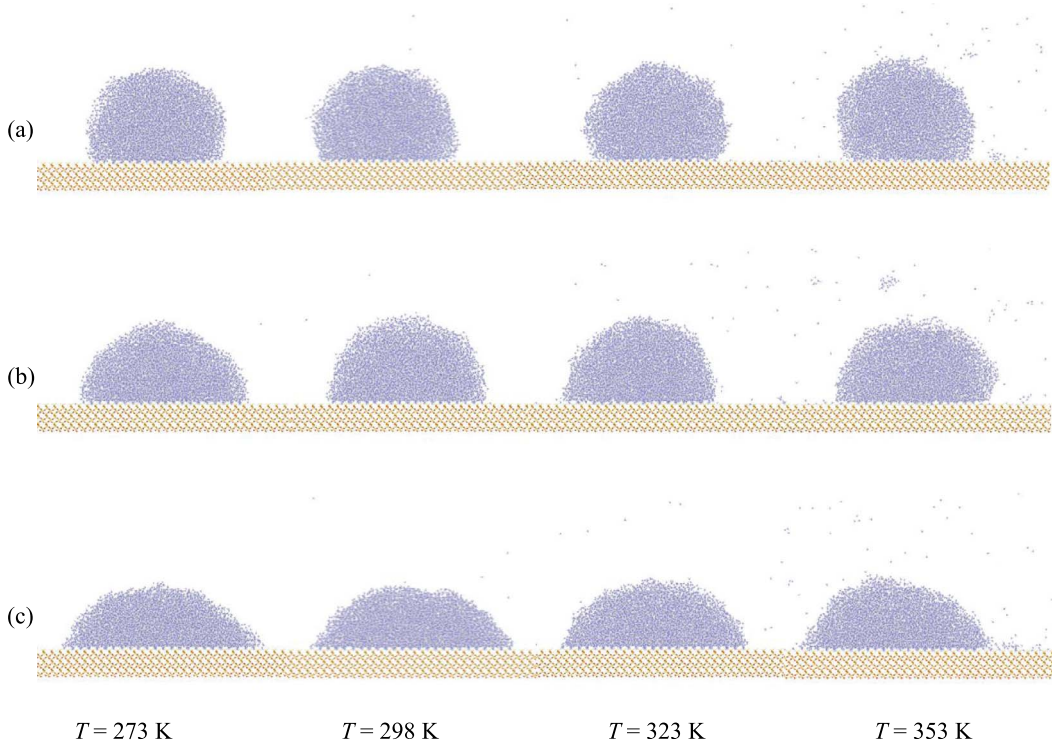

Figure 9. Snapshots of simulation systems at the equilibrium state for various temperatures, (a) ε_{Si} = 0.008 kcal/mol; (b) ε_{Si} = 0.4 kcal/mol; (c) ε_{Si} = 0.8 kcal/mol.

3.3. *Effect of temperature*

Considering that the influence of temperature on the wettability may be affected by the hydrophobicity or hydrophilicity of the silica surface, three representative interaction potential energies including 0.008 (hydrophobic surface), 0.4 (neutral surface), and 0.8 (hydrophilic surface) kcal/mol are adopted in this simulation. Moreover, the simulations are carried out at different temperatures of 273 K, 298 K, 323 K, and 353 K to investigate the influence of temperature on wettability.

The snapshots of simulation systems at the equilibrium state for various temperatures are shown in Figure 9. The molecular diffusions increase with temperature, especially for the hydrophobic surface (ε_{Si} = 0.008 kcal/mol), which implies that interaction potential energy is small and easy to be disturbed by the diffusion effect, leading to a looser and more flexible water structure. Figure 10 shows the water contact angle calculated by the same approach as the last section. As predicted before, the influence of temperature on wettability is veritably impacted by the hydrophobicity or hydrophilicity of the silica surface. For hydrophobic and neutral surfaces (ε_{Si} = 0.008, 0.4 kcal/mol), the contact angles increase slightly, whereas they increase significantly for the hydrophilic surface. It can be explained that the repulsive force from the silica surface increases with temperature and is greater than the interaction between water molecules.

Vapor–liquid interface thickness and the total droplet height can be obtained by one-dimensional density profiles as shown in Tables 4 and 5, respectively. As can be seen, with the increase of temperature, the total droplet heights and vapor–liquid interface thicknesses gradually increase for the three types of the silica surface, proving the mechanism of contact angles. It is interesting to note that the increased amplitudes of total droplet height and vapor–liquid interface

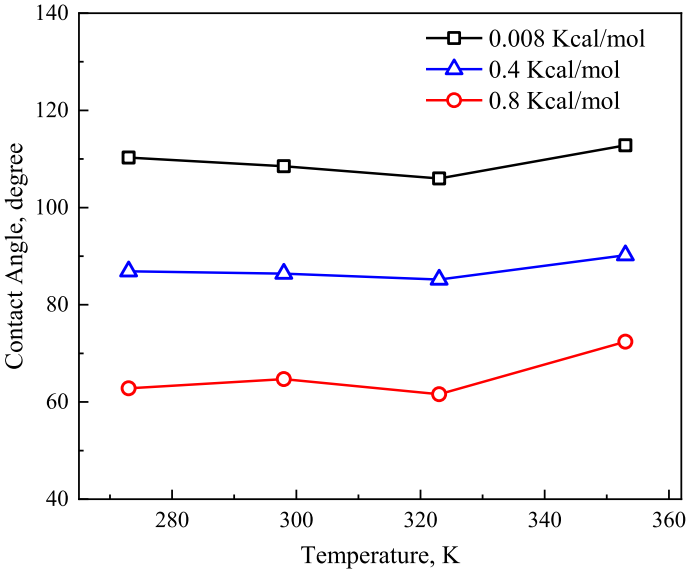

Figure 10. Changes of contact angles under different temperatures.

Table 4. Total droplet height of various temperatures (h/Å)

Temperatures T/K	273	298	323	353
$\varepsilon_{Si} = 0.008$ kcal·mol^{-1}	76.5	73.5	80.5	82
$\varepsilon_{Si} = 0.4$ kcal·mol^{-1}	59	57.5	60.5	61.5
$\varepsilon_{Si} = 0.8$ kcal·mol^{-1}	55.5	53.5	56.5	63

Table 5. Vapor–liquid interface thickness of various temperatures (d/Å)

Temperatures T/K	273	298	323	353
$\varepsilon_{Si} = 0.008$ kcal·mol^{-1}	3.5	2.5	3	4.5
$\varepsilon_{Si} = 0.4$ kcal·mol^{-1}	2.5	3.5	5	6.5
$\varepsilon_{Si} = 0.8$ kcal·mol^{-1}	2.5	3.5	6	11

thickness are larger for the hydrophilic surface. According to the counterbalance between surface tension and the absorption of water and silica wall, it can be explained that the surface tension dissipates more energy than the absorption of water molecules in the higher temperature, so that surface tension rejects more water molecules, enlarging the contact angle and total droplet height, vice versa. Vapor–liquid interface thickness demonstrates the diffusion between liquid and gas, and surfaces for high interaction potential energy have strong molecule absorption or rejection, so the diffusion effect for the hydrophilic surface is also susceptible to temperature.

4. Conclusions

The wettability of nano water droplets on the silica surface has been investigated by means of MD simulation. Snapshots, time average density profiles, one-dimensional density files for simulation systems in equilibrium states are obtained to calculate the contact angles, nano water droplet heights, and vapor–liquid interface thicknesses. To determine the simulation parameters,

eight groups of simulation systems for various thicknesses and widths (lengths) of silica substrate are carried out first, and the results show little effect on contact angle. Further study on 17 groups of simulation systems for interaction potential energies (ε_{Si} = 0.008, 0.04, 0.2, 0.4, 0.6, 0.8, 1, 2 kcal/mol) and temperatures (T = 273, 298, 323, 353 K) are conducted. It is observed that the contact angles vary intensively with interaction potential energies from 108.5° to 18.1°, which implies a transition from hydrophobic to hydrophilic. It can be concluded that an increase in the interaction potential energy will enhance wettability. Results of simulations for various temperatures show that the contact angle increase with temperature, whatever the hydrophobic or hydrophilic of the silica surface.

It is noted that the results cannot be completely consistent with the experimental research on the macroscopic scale due to the small size effect of nano water droplets. Future work should be conducted to connect the perspectives of microscopic and macroscopic and further investigate the multi-scale wetting process.

Acknowledgments

This research is supported by the National Natural Science Foundation of China (No. 51878665). This work is supported in part by the High Performance Computing Center of Central South University.

References

[1] W. J. Likos, N. Lu, "Hysteresis of capillary cohesion in unsaturated soils", in *15th ASCE Engineering Mechanics Conference, June 2–5, 2002*, Columbia University, New York, NY, 2002.

[2] D. Gallipoli, A. Gens, R. Sharma, J. Vaunat, "An elasto-plastic model for unsaturated soil incorporating the effects of suction and degree of saturation on mechanical behavior", *Géotechnique* **53** (2003), no. 1, p. 123-136.

[3] Y. H. Zhang, "Study on the early warning value of slope slide collapse induced by rainfall in weihong railway", *Railway Construct.* **11** (2013), p. 83-86.

[4] S. Zhang, J. Teng, Z. He, Y. Liu, S. Liang, Y. Yao, D. Sheng, "Canopy effect caused by vapour transfer in covered freezing soils", *Géotechnique* **66** (2016), no. 11, p. 927-940.

[5] H. J. Butt, D. S. Golovko, E. Bonaccurso, "On the derivation of Young's equation for sessile drops: None equilibrium effects due to evaporation", *J. Chem. Phys.* **111** (2007), no. 19, p. 5277-5283.

[6] B. Straughan, "Surface -tension -driven convection in a fluid overlying a porous layer", *J. Comput. Phys.* **170** (2001), no. 1, p. 320-337.

[7] J. Teng, F. Shan, Z. He, S. Zhang, G. Zhao, D. Sheng, "Experimental study of ice accumulation in unsaturated clean sand", *Géotechnique* **69** (2019), no. 3, p. 251-259.

[8] W. L. Qiang, B. H. Wang, Z. J. Yu, "Molecular dynamics simulation of wetting and liquid-vapor interface characteristics of sessile nano liquid droplets", *Henan Chem. Ind.* **9** (2017), p. 18-22.

[9] J. D. Teng, J. Y. Kou, X. D. Yan, S. Zhang, D. C. Sheng, "Parameterization of soil freezing characteristic curve for unsaturated soils", *Cold Reg. Sci. Technol.* **170** (2020), no. 68, article no. 102928.

[10] L. M. Arya, J. F. Paris, "A physicoempirical model to predict the soil-moisture characteristic from particle-size distribution and bulk-density data", *Soil Sci. Soc. Am. J.* **45** (1981), no. 6, p. 1023-1030.

[11] J. Bachmann, R. R. Van der Ploeg, "A review on recent developments in soil water retention theory: interfacial tension and temperature effects", *J. Plant Nutr. Soil Sci.* **165** (2002), no. 4, p. 468-478.

[12] D. G. Fredlund, A. Q. Xing, S. Y. Huang, "Predicting the permeability function for unsaturated soils using the soil–water characteristic curve", *Can. Geotech. J.* **31** (1994), no. 4, p. 533-546.

[13] Y. F. Fattah, F. J. Kadhim, "Consolidation characteristics of unsaturated soil", *Eng. Tech. J.* **27** (2009), no. 10, p. 2027-2046.

[14] T. Chau, "A review of techniques for measurement of contact angles and their applicability on mineral surfaces", *Miner. Eng.* **22** (2009), no. 3, p. 213-219.

[15] A. Adamson, A. Gast, *Physical Chemistry of Surfaces*, John Wiley & Sons, New York, 1997.

[16] J. Bachmann, S. K. Woche, M. O. Goebel, M. B. Kirkham, R. Horton, "Extended methodology for determining wetting properties of porous media", *Water Resour. Res.* **39** (2003), no. 12, p. 1353.

[17] A. F. Stalder, G. Kulik, D. Sage, L. Barbieri, P. Hoffmann, "Asnake-based approach to accurate determination of both contact points and contact angles", *Colloids Surf. A: Physicochem. Eng. Asp.* **286** (2006), no. 1, p. 92-103.

[18] Y. Y. Zuo, C. Do, A. W. Neumann, "Automatic measurement of surface tension from noisy images using a component labeling method", *Colloids Surf. A: Physicochem. Eng. Asp.* **299** (2007), no. 1, p. 109-116.
[19] A. F. Stader, T. Melchior, M. Muller, D. Sage, T. Blu, M. Unser, "Low-bond axisymmetric drop shape analysis for surface tension and contact angle measurements of sessile drops", *Colloids Surf. A: Physicochem. Eng. Asp.* **364** (2010), no. 1, p. 72-81.
[20] J. Y. Shang, M. Flury, J. B. Harsh, R. L. Zollars, "Contact angles of aluminosilicate clays as affected by relative humidity and exchangeable cations", *Colloids Surf. A Physicochem. Eng. Asp.* **353** (2010), no. 1, p. 1-9.
[21] D. Sergi, G. Scocchi, A. Ortona, "Molecular dynamics simulations of the contact angle between water droplets and graphite surfaces", *Fluid Phase Equilib.* **332** (2012), p. 173-177.
[22] W. Xu, Z. Lan, B. L. Peng, R. F. Wen, X. H. Ma, "Molecular dynamics simulation on the wetting characteristic of micro-droplet on surfaces with different free energies", *Acta Phys. Sin.* **64** (2015), no. 21, p. 374-381.
[23] C. D. Wu, L. M. Kuo, S. J. Lin, T. H. Fang, S. F. Hsieh, "Effects of temperature, size of water droplets, and surface roughness on nanowetting properties investigated using molecular dynamics simulation", *Comput. Mater. Sci.* **53** (2012), no. 1, p. 25-30.
[24] D. Niu, G. H. Tang, "Static and dynamic behavior of water droplet on solid surfaces with pillar-type nanostructures from molecular dynamics simulation", *Int. J. Heat Mass Transf.* **79** (2014), p. 647-654.
[25] W. J. Jeong, M. Y. Ha, H. S. Yoon, M. Ambrosia, "Dynamic behavior of water droplets on solid surfaces with pillar-type nanostructures", *Langmuir* **28** (2012), no. 12, p. 5360-5371.
[26] M. S. Ambrosia, M. Y. Ha, S. Balachandar, "The effect of pillar surface fraction and pillar height on contact angles using molecular dynamics", *Appl. Surf. Sci.* **282** (2013), p. 211-216.
[27] J. R. Hill, C. M. Freeman, L. Subramanian, "Use of force fields in materials modeling", *Rev. Comput. Chem.* **16** (2000), p. 141-216.
[28] B. Vessal, "Simulation studies of silicates and phosphates", *J. Non-Cryst. Solids* **177** (1994), p. 103-124.
[29] J. R. Hill, J. Sauer, "Molecular mechanics potential for silica and zeolite catalysts based on ab initio calculations. 1. Dense and microporous silica", *J. Phys. Chem.* **98** (1994), no. 4, p. 1238-1244.
[30] J. R. Hill, J. Sauer, "Molecular mechanics potential for silica and zeolite catalysts based on ab initio calculations. 2. Aluminosilicates", *J. Phys. Chem.* **99** (1995), no. 23, p. 9536-9550.
[31] K. P. Schröder, J. Sauer, "Potential functions for silica and zeolite catalysts based on ab initio calculations. 3. A shell model ion pair potential for silica and aluminosilicates", *J. Phys. Chem.* **100** (1996), no. 26, p. 11043-11049.
[32] W. G. Hoover, "Canonical dynamics: equilibrium phase-space distributions", *Phys. Rev. A (Gen. Phys.)* **31** (1985), no. 3, p. 1695-1697.
[33] S. D. Hong, M. Y. Ha, S. Balachandar, "Static and dynamic contact angles of water droplet on a solid surface using molecular dynamics simulation", *J. Colloid Interface Sci.* **339** (2009), no. 1, p. 187-195.
[34] F. F. Cun, C. Tahir, "Wetting of crystalline polymer surfaces: a molecular dynamics simulation", *J. Phys. Chem.* **103** (1995), no. 20, p. 9053-9053.
[35] D. W. Heermann, "Computer-simulation method", in *Computer Simulation Methods in Theoretical Physics*, Springer, Berlin, Heidelberg, 1990.
[36] P. Adams, J. R. Henderson, "Molecular dynamics simulations of wetting and drying in LJ models of solid-fluid interfaces in the presence of liquid-vapour coexistence", *Mol. Phys.* **73** (1991), no. 6, p. 1383-1399.
[37] T. Werder, J. H. Walther, R. L. Jaffe, T. Halicioglu, P. Koumoutsakos, "On the water-carbon interaction for use in molecular dynamics simulations of graphite and carbon nanotubes", *J. Phys. Chem. B* **107** (2003), p. 1345-1352.
[38] G. C. Cho, J. C. Santamarina, "Unsaturated particulate materials–particle-level studies", *J. Geotech. Geoenviron. Eng.* **127** (2001), no. 1, p. 84-96.
[39] S. Leroch, M. Wendland, "Influence of capillary bridge formation onto the silica nanoparticle interaction studied by grand canonical monte carlo simulations", *Langmuir* **29** (2013), no. 40, p. 12410-12420.
[40] C. M. Tenney, R. T. Cygan, "Molecular simulation of carbon dioxide, brine, and clay mineral interactions and determination of contact angles", *Environ. Sci. Technol.* **48** (2014), no. 3, p. 2035-2042.
[41] T. Y. Zhao, P. R. Jones, N. A. Patankar, "Thermodynamics of sustaining liquid water within rough icephobic surfaces to achieve ultra-low ice adhesion", *Sci. Rep.* **9** (2019), article no. 258.
[42] M. J. de Ruijter, T. D. Blake, J. De Coninck, "Dynamic wetting studied by molecular modeling simulations of droplet spreading", *Langmuir* **15** (1999), p. 7836-7847.
[43] E. B. Moore, J. T. Allen, V. Molinero, "Liquid-ice coexistence below the melting temperature for water confined in hydrophilic and hydrophobic nanopores", *J. Phys. Chem. C.* **116** (2012), p. 7507-7514.
[44] J. K. Singh, F. Müller-Plathe, "On the characterization of crystallization and ice adhesion on smooth and rough surfaces using molecular dynamics", *Appl. Phys. Lett.* **104** (2014), article no. 021603.
[45] S. Xiao, J. He, Z. Zhang, "Nanoscale deicing by molecular dynamics simulation", *Nanoscale* **8** (2016), p. 14625-14632.
[46] C. Zhang, Z. Liu, P. Deng, "Contact angle of soil minerals: A molecular dynamics study", *Comput. Geotech.* **75** (2016), p. 48-56.